JOURNAL OF CATALYSIS **171,** 27–44 (1997)
ARTICLE NO. CA971769

Kinetic and Mechanistic Study of NO_x Reduction by NH_3 over H-Form Zeolites

II. Semi-Steady-State and *In Situ* FTIR Studies

John Eng and Calvin H. Bartholomew

BYU Catalysis Laboratory, Brigham Young University, Provo, Utah 84602

Received August 12, 1996; revised March 27, 1997; accepted June 4, 1997

A series of transient kinetic, semi-steady-state kinetic and *in situ* Fourier transform infrared spectroscopy (FTIR) experiments were conducted using NH_3-presorbed H-form pentasil zeolites to reduce NO_x to N_2. Semi-steady-state kinetic experiments were performed at temperatures below 210°C to determine reaction rate parameters for the reduction of NO over NH_3-presorbed H-mordenite. Transient test results suggest that pairs of NH_3 molecules adsorbed onto neighboring acid sites are necessary for NO reduction to N_2. Results of *in situ* FTIR experiments were used to identify the structures of adsorbed NH_3 and intermediate NO_x species. These FTIR results suggest that adsorbed NH_3 is most reactive when it is bonded to the Brønsted acid sites in zeolites through three hydrogen bonds. *In situ* FTIR spectra also indicate that an NO_2-type intermediate is formed on the zeolite surface during selective catalytic reduction (SCR). Formation of this NO_2-type species appears to be a necessary step in the SCR reaction mechanism as the concentration of adsorbed NH_3 does not decrease (i.e., react) until a band corresponding to this NO_2-type species appears. Combined analyses of transient and *in situ* FTIR results were used to develop a reaction mechanism which describes NO or NO_2 reduction by NH_3 over H-form zeolites.

INTRODUCTION

Hydrogen and metal-exchanged zeolites have uniquely high activities and selectivities for selective catalytic reduction (SCR) of NO_x with NH_3 or hydrocarbon reducing agents. Their catalytic properties are probably a consequence of the unique environment of cationic sites in spatially confined pores of zeolites leading to unusual interactions between reactants and catalytic sites. For instance, it has been postulated that (i) the zeolite exerts an important electronic effect in Co^{2+} activation in NO_x reduction with CH_4 over Co-ZSM-5 and Co-mordenite (1), (ii) the function of the zeolite is to stabilize reactive intermediates (2), and (iii) acid sites are active sites in NO reduction with hydrocarbons (3, 4). Nevertheless, the nature of molecular and cation interactions with zeolites is not well understood. A clearer understanding of the reactions occurring on H-form zeolites during SCR should aid in understanding the promoting effect of exchanged cations. In addition, mechanistic information may also reveal issues regarding zeolite structure which are essential for high SCR activity in zeolite-based catalysts. Therefore, an understanding of the SCR reaction mechanism on H-form zeolites may provide an important foundation for the development of more active zeolite-based SCR catalysts.

Three previously reported studies specifically address the mechanism of SCR of NO with NH_3 on H-zeolites. Kiovsky *et al.* (5) suggested that NO_2 is the active intermediate in the SCR of NO_x over H-mordenite. Interestingly, Hamada *et al.* (6) and Sasaki *et al.* (7) also concluded NO_2 to be the active intermediate in the SCR of NO_x with propane over H-ZSM-5. Similarly, Yogo *et al.* (8) suggested that NO_2 plays an important role in the selective reduction of NO by CH_4 over H-form zeolites. Each of these workers observed that increasing the NO_2/NO ratio in the reactant stream increases the overall rate of NO_x reduction. In SCR with metal-exchanged zeolites, NO_2 has also been suggested as an active intermediate (1, 9–13).

Andersson and co-workers (14–16), however, suggested a mechanism for SCR of NO by NH_3 on H-mordenite involving NO oxidation (by O_2 or NO_2) to nitrosonium ions, NO^+. Moreover, they correlated NO^+ adsorbance to first order reaction rate constants for a range of dealuminated H-mordenite samples. NO^+ absorbance, however, was determined by adsorbing NO at 650 K followed by infrared measurements at room temperature. Thus, there was no direct evidence that NO^+ species participate in SCR reactions.

Ito *et al.* (17), in their studies of NO reduction by NH_3 over CeNa-mordenite (which they compared to H-mordenite), suggested a combination of the two mechanisms proposed above. They found their data to be more consistent with NO oxidation to NO_2 at 300°C and NO oxidation to NO^+ at 510°C.

0021-9517/97 $25.00

Thus, in summarizing the previous work, there is no consensus regarding the mechanism of SCR of NO by NH_3; the results are consistent with either an NO_2 or NO^+ intermediate.

Evidence to distinguish between the two proposed intermediates (i.e., NO_2 or NO^+) can be obtained from *in situ* tests which monitor the presence of adsorbed species during SCR. For instance, identification of active intermediate species for various reactions can be performed using Fourier transform infrared spectroscopy (FTIR). Difficulties can arise, however, when attempting to utilize this technique for high-temperature SCR reactions. High-temperature *in situ* detection of intermediate species is often difficult or impossible due to the small concentrations of adsorbed species present at high temperatures. Indeed, *in situ* FTIR experiments performed in our laboratory at temperatures above 300°C with NO, O_2, and NH_3 reacting over H-ZSM-5 did not have the sensitivity to enable detection of any adsorbed NO_x species. In view of such difficulties, many workers have investigated the nature of intermediate species by performing FTIR experiments of adsorbed species at lower temperatures (at which reaction rates are low) and thereby make inferences regarding the nature of species which may be involved at higher temperatures (15, 18–20).

Results of our earlier kinetic study (21) provide evidence that NO reacts with O_2 to form an active intermediate species which adsorbs and subsequently reacts with adsorbed NH_3. In addition, adsorbed NH_3 must have been present for adsorption of the active NO_x species to occur. Identification of the adsorbed species, however, could not be made from the kinetic and transient tests performed in our previous study. An additional observation was that gaseous NH_3 inhibits the SCR reaction by limiting access of the active NO_x species to adsorption sites within the zeolite. Based upon these observations, it was determined that SCR of NO_x with NH_3 could be carried out more effectively by presorbing NH_3 onto an H-form zeolite and then exposing the NH_3-presorbed zeolite to the NO_x-containing stream. Initial tests confirmed that SCR operation in this manner not only increased reaction rates at high temperatures, but also enabled operation with considerable activity at temperatures as low as 125°C. Since reactions could be carried out at lower temperatures with this approach, higher concentrations of adsorbed intermediate species would facilitate their detection using *in situ* FTIR experiments.

In this study, semi-steady-state kinetic tests, transient kinetic tests and *in situ* FTIR studies were performed to investigate the nature of active intermediates present during reaction and the types of sites upon which these intermediates adsorb. Based upon results of this study, issues regarding the influence of zeolite structure are addressed and suggestions are provided to explain the promoting effect of metal exchange in zeolite-based SCR catalysts. Semi-steady-state kinetic experiments were performed at temperatures below 210°C to determine reaction rate parameters for the reduction of NO over NH_3-presorbed H-mordenite. *In situ* FTIR experiments were used to identify the structures of adsorbed NH_3 and intermediate NO_x species. Analyses of transient kinetic and *in situ* FTIR experimental results were combined to develop a reaction mechanism for NO_x reduction by NH_3 over H-form zeolites.

EXPERIMENTAL

Samples of NH_4-Z-12 were obtained from Tosoh USA, and samples of H-Z-21, Na-Z-26, Na-Z-35, Na-M-5, NH_4-M-10, and H-Y-2.5 were obtained from the PQ Corporation (where Z, M and Y refer to ZSM-5, mordenite, and Y-zeolite, respectively, and the last number in each sample indicates the Si/Al ratio). Conversion of samples to H-form zeolites are described in a previous paper (21).

Scanning electron microscopy (SEM) was performed using a JEOL JSM-840A scanning electron microscope. Powdered samples were prepared for SEM analysis by placing them in an E5300 freeze-dryer with sputtering attachment and gold was deposited for 3 min at 18–20 mA (leaving a gold coat of approximately 200 Å). Surface area measurements were performed on a Micromeritics Gemini 2360 surface area analyzer. Approximately 0.25 g powdered samples were placed in the instrument and surface areas were calculated using standard BET analysis of N_2 adsorption data.

Transient and semi-steady-state kinetic tests were performed using calibration quality NO, NO_2, and NH_3 gases diluted in He (Matheson) introduced without further purification. Ultra-high-purity He was further purified using Cu-deoxygenation and molecular sieve traps. O_2 (10.3% in He from Matheson Gas) was also dried by passing it through a molecular sieve trap. H_2O was added during semi-steady-state kinetic tests by passing He through a controlled-temperature water bath just prior to mixing with all other reactant gases before injection into the reactor cells. Due to the use of teflon flow lines, heat tracing was not employed, which limited the maximum concentration of H_2O which could be used.

Transient tests involving NH_3 presorption were performed using the same temperature-programmed desorption (TPD) apparatus described previously (21) by presorbing NH_3 onto H-form zeolite samples at reaction temperatures, purging the samples with He, and subsequently admitting NO and O_2 to the catalyst. The effluent gas composition was continuously monitored using a UTI100C quadrapole mass spectrometer.

In order to perform continuous semi-steady-state kinetic tests, a "rotating flow" reactor setup (shown schematically in Fig. 1) was designed and constructed. Teflon flow lines were used to minimize complications due to NO/NO_2 adsorption on stainless steel lines. In this setup, all four

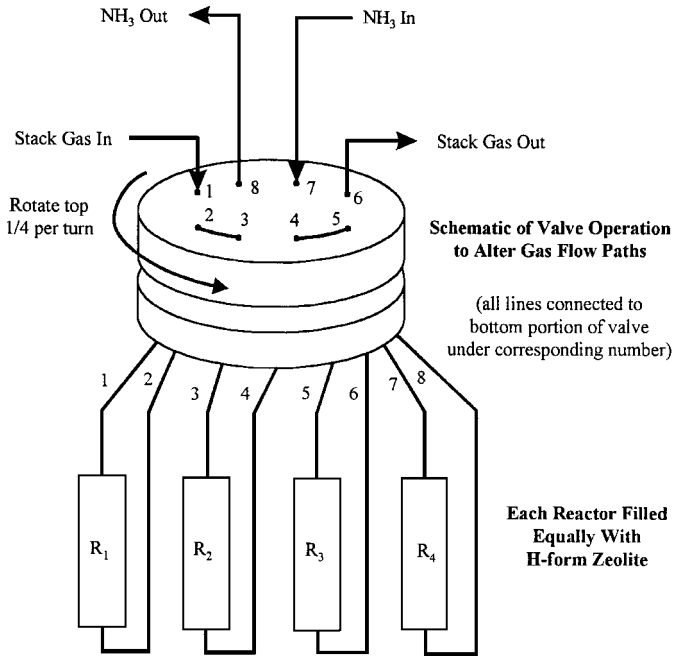

FIG. 1. Schematic of "rotating flow" reactor for semi-steady-state kinetics studies.

reactors were loaded with equal amounts of an H-form zeolite. During operation, one of the four reactors was injected with NH_3 while the NO_x-containing stream was fed through the other three reactors connected in series. In this manner, beds of NH_3-presorbed catalyst were continually replenished to overcome limitations imposed by the NH_3 storage capacities of zeolites. During a rotation cycle, the bed into which NH_3 had been most recently injected was the first bed into which stack gases were injected. Analyses of the effluent gases were performed using a UTI100C mass spectrometer, an HP 5810 gas chromatograph equipped with a thermal conductivity detector for N_2 and N_2O measurements and a Rosemount chemiluminescence NO_x analyzer for continuous NO and NO_2 detection.

FTIR spectra were collected on a Nicolet 730 FTIR spectrometer equipped with a liquid N_2-cooled MCT detector. H-ZSM-5 samples were pressed at 10,000 psi for 2 min into self-supporting wafers, while H-mordenite samples were pressed at 15,000 psi. The wafers were loaded into a stainless-steel cell sealed with CaF_2 windows. The cell could be heated up to 500°C. Background spectra were obtained by accumulating 100 scans at a spectral resolution of 4 cm^{-1}, while all other spectra were obtained using 32 scans.

RESULTS

SEM and surface area tests. Scanning electron micrographs of each of the mordenite and ZSM-5 powder samples are shown in Fig. 2. In each case, average crystallite sizes range between approximately 1 and 7 μm. Larger particles consist of aggregates of these small crystallites. Surface areas measured by BET analysis for each of the zeolites are 300–400 m^2/g.

Transient tests utilizing NH_3 presorption. Based upon our previous studies which suggested an inhibition effect by gas-phase NH_3, it was postulated that NO reduction could be enhanced by presorbing with NH_3. Indeed, tests performed by presorbing NH_3 onto H-Z-12, H-Z-26, and H-M-5 followed by admission of flowing NO and O_2 confirmed this hypothesis. Figure 3 displays the transient NO, N_2, and H_2O concentration profiles obtained as 3000 ppm NO and 4% O_2 in He were passed over H-M-5 (GHSV = 30,000) at 291°C which had been previously treated with NH_3 at the same temperature. The rate of N_2 formation at 291°C, which is proportional to the concentration of N_2 formed, reaches a maximum value of 1.4×10^{-6} $mol/g_{cat} \cdot s$, which is greater than the rate of 0.4×10^{-6} $mol/g_{cat} \cdot s$ observed when coinjecting the same reactants at 425°C (21). By comparison, negligible SCR rates were observed when NO, O_2, and NH_3 were coinjected at temperatures below 300°C (21). Thus, higher rates of reaction are achieved by NH_3 presorption followed by reaction with NO and O_2. Figure 3 also illustrates that the removal of NO is accompanied by increases in N_2 and H_2O concentration. The decrease in NO concentration exceeds the corresponding increase in N_2 concentration; however, adsorption of NO (which does not instantaneously form N_2) may contribute to this difference. Evidence of additional NO adsorption is also observed after N_2 formation ceases (i.e., [NO] does not return to 3000 ppm). Comparison of the quantities of N_2 and H_2O formed due to reaction yields a molar ratio of approximately $1.5H_2O/N_2$ which is consistent with an overall stoichiometry of

$$4NO + 4NH_3 + O_2 \rightarrow 4N_2 + 6H_2O. \quad [1]$$

It should be noted, however, that since accurate calibration gas standards containing ppm levels of H_2O in He were not available, the calibration constant previously obtained for NH_3 was used for calculating H_2O concentration. Thus, the measured H_2O/N_2 molar ratio is only approximate.

Another interesting feature of the transient concentration profiles is that minimum NO and maximum N_2 concentrations are not reached immediately. Since the high space velocities used should result in immediate concentration changes throughout the reactor (i.e., within seconds), the relatively slow decrease in NO concentration with time indicates that catalyst activation occurs over the first few minutes of reaction. This observation suggests that active species or complexes must be formed before maximum rates of NO reduction can be attained. Since adsorbed NH_3, NO, and O_2 are necessary for N_2 formation to occur (21), the active complex likely consists of NH_3, NO, and O_2. The nature of this active complex is discussed further in conjunction with results of FTIR experiments.

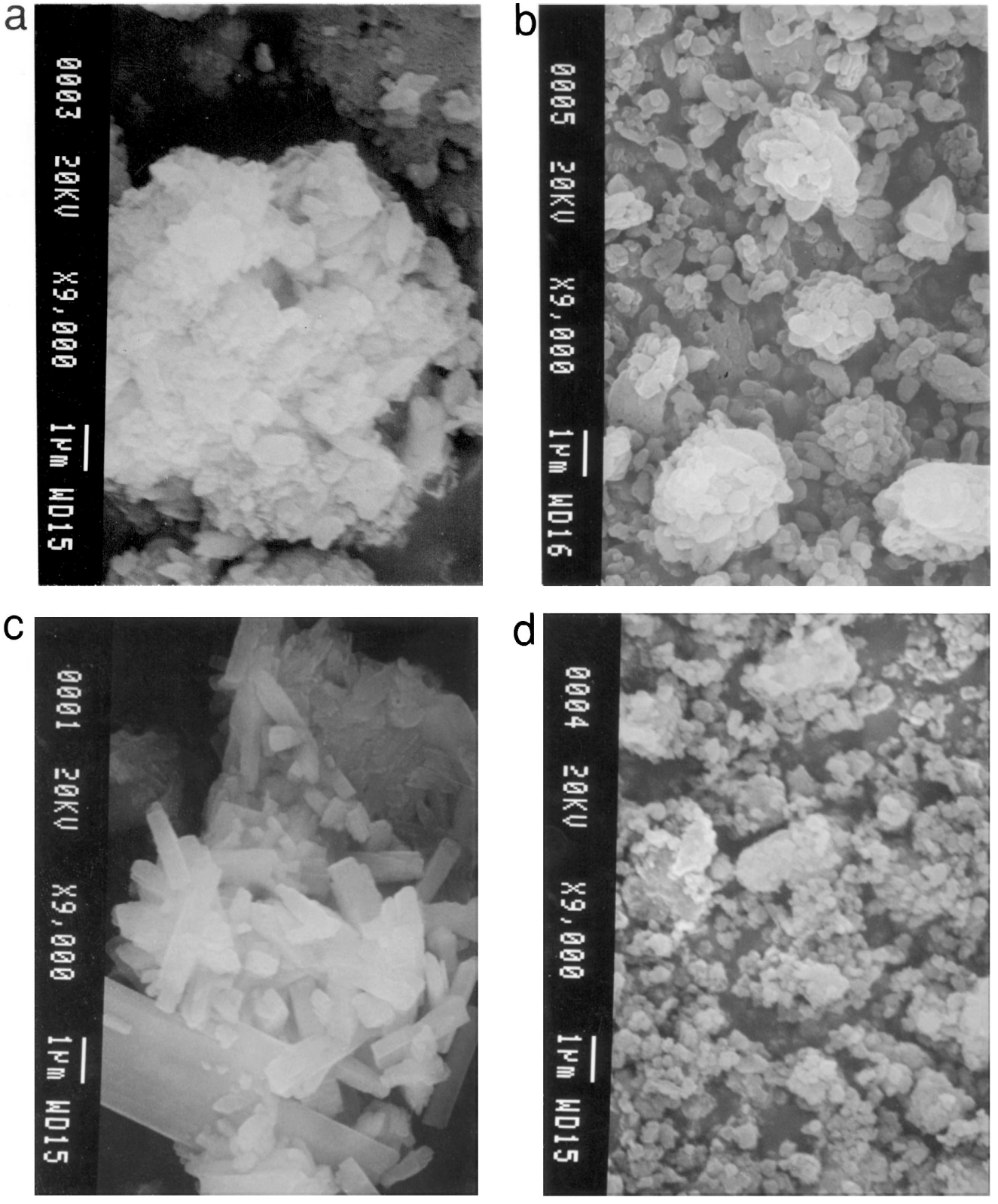

FIG. 2. SEM micrographs (original magnification×9000) of H-form zeolites (a) H-M-5, (b) H-M-10, (c) H-Z-12, (d) H-Z-21, (e) H-Z-26, and (f) H-Z-35.

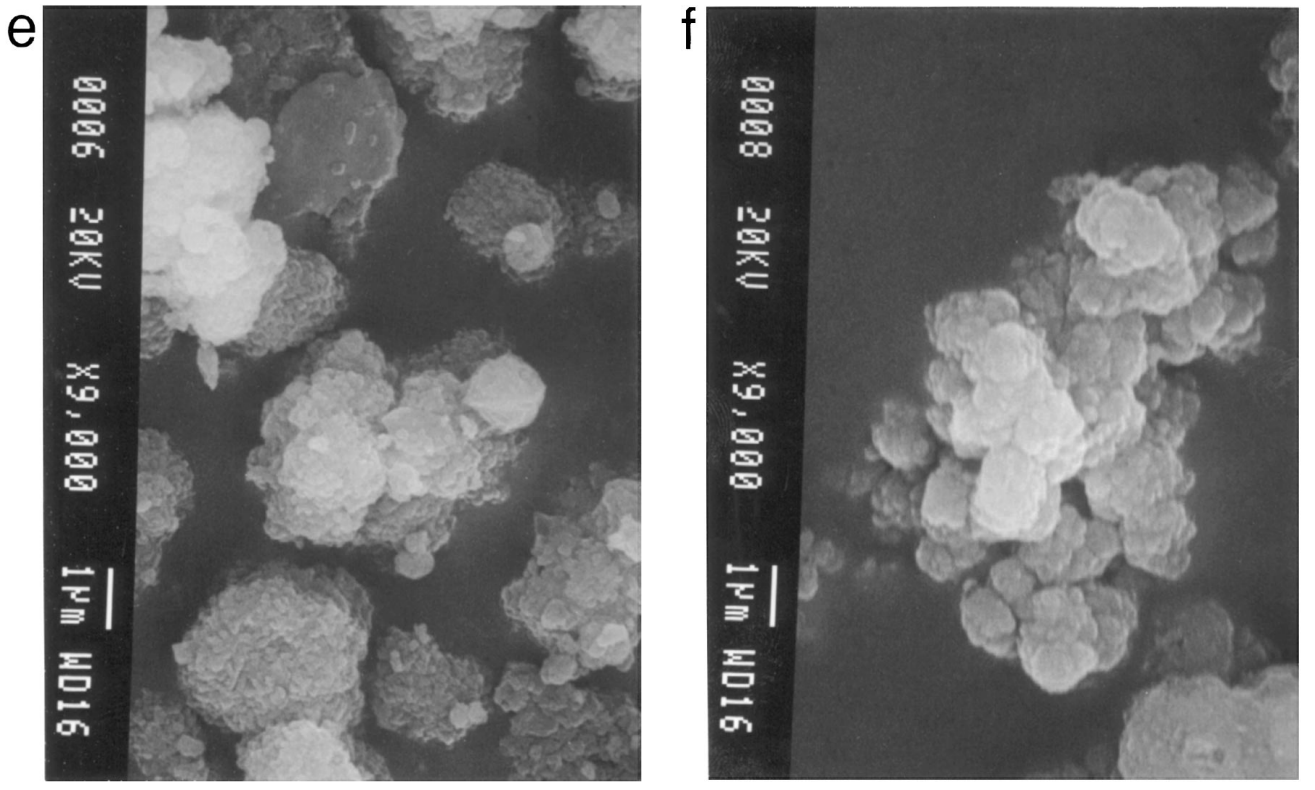

FIG. 2—*Continued*

N_2 formation rates obtained in transient experiments over H-Z-12, H-Z-26, and H-M-5 are compared in Fig. 4. Each of the profiles shown occurred in response to the admission of 1000 ppm NO and 1.5% O_2 in He (150 cm^3/min) to NH_3-presorbed samples (104–188 mg) of H-form zeolites at 325°C. In each case, an activation period, similar to that shown in Fig. 3, is observed. While the duration of the reaction period varies according to the NH_3 storage capacity of each zeolite, maximum rates of N_2 formation are the same independent of zeolite type and acid site concentration for these pentasils of high aluminum content. However, this observation cannot be generalized to any zeolite structure and aluminum content.

In fact, when the same transient tests were performed with H-M-10, H-Z-35, or H-Y-2.5, negligible N_2 formation was observed. These results confirm previous findings that these same zeolites are inactive in conventional steady-state SCR (21) and suggest that a threshold Si/Al ratio exists, below which the catalyst is active. Moreover, the threshold Si/Al ratio for a zeolite to be active as an SCR catalyst is dependent upon the zeolite type with higher Al contents

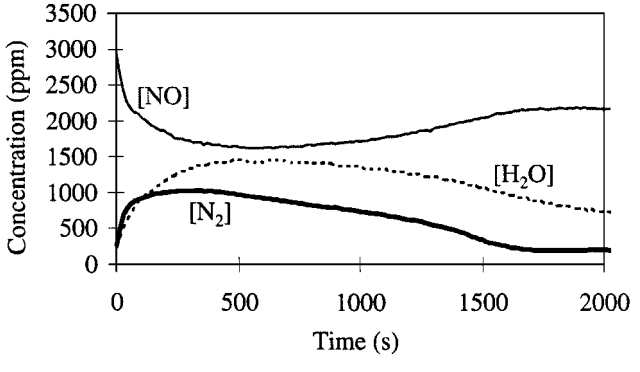

FIG. 3. Transient NO, N_2, H_2O concentration profiles observed while passing 3000 ppm NO, and 4% O_2 at 291°C over H-M-5 containing NH_3 preadsorbed at 291°C (GHSV = 30,000 h^{-1}).

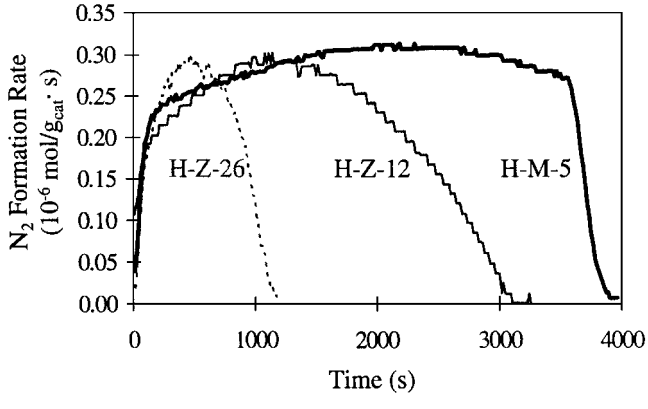

FIG. 4. Comparison of N_2 formation rates observed while passing 1000 ppm NO, and 1.5% O_2 at 325°C over H-Z-12, H-Z-26, and H-M-5 containing NH_3 preadsorbed at 325°C.

required for mordenite (Si/Al = 5) as compared with H-ZSM-5 (Si/Al = 26). The finding that H-Y (Si/Al = 2.5) is also inactive, despite its high acid site concentration, is also a reflection of the importance of zeolite structure on SCR activity.

Integration of the curves displayed in Fig. 4 enables calculation of the total amounts of N_2 formed over each of the NH_3-presorbed catalysts. These calculations reveal that quantities of N_2 formation over the three zeolites decrease in the order H-M-5 > H-Z-12 > H-Z-26 with integrated values of 929, 591, and 212 μmol/g, respectively. Relative to their total Al contents (as calculated from their respective Si/Al ratios), these values yield N_2/Al ratios of only 0.34, 0.46, and 0.34 for H-M-5, H-Z-12, and H-Z-26, respectively. If each Al atom is associated with an acid site onto which NH_3 is adsorbed, these ratios indicate that less than half of the adsorbed NH_3 in H-mordenite or H-ZSM-5 contributes to the formation of N_2.

Semi-steady-state-kinetic tests. Semi-steady-state tests were first performed by adsorbing NH_3 and reacting NO in separate reactors (as described under Experimental) at temperatures above 270°C. Effluent NO_x concentrations were recorded and N_2 concentrations were measured at the end of each cycle (i.e., just prior to flow switching). Since transient tests indicate that NO adsorbs and/or reacts with other adsorbed species, data are reported in terms of NO_x removal levels which account for both NO_x conversion to N_2 and NO_x adsorption. As illustrated in Table 1, NO_x removal levels greater than 93% are obtained over H-M-5 (1% < O_2 < 4%, GHSV = 15,000). Comparisons between NO removal levels and N_2 formation rates indicate that approximately 1 molecule of N_2 is formed for each molecule of NO removed. Stoichiometrically, this suggests that one adsorbed NH_3 molecule is capable of reducing one NO molecule to form one N_2 molecule as given by the stoichiometry in reaction [1]. Cycle times were specified by assuming a 1:1 NO/NH_3 stoichiometry and adsorption of one NH_3 molecule per Al atom in the zeolite sample to calculate the total amount of NH_3 introduced during each cycle. Reductions in cycle time did not affect NO removal trends since the amount of NH_3 introduced per cycle exceeded the amount of NO to be removed per cycle. However, increases in the cycle times resulted in rapid decreases in NO conversion at the end of each cycle due to depletion of reactant NH_3. This confirms that NH_3 adsorbed onto sites associated with Al atoms in zeolites are active for NO removal. Moreover, these results indicate that each NH_3 molecule associated with an Al atom is capable of removing one NO molecule to form one N_2 molecule. However, this is apparently inconsistent with results of the transient tests (described previously) which indicate that not all acid sites are active for producing N_2.

TABLE 1

Semi-Steady-State Kinetic Data Obtained over H-M-5 (Q = 150 cm^3/min)

T (°C)	W (g)	[H_2O] (%)	[O_2] (%)	[NO] in (ppm)	[NO_x] out (ppm)	NO_x removal
274	0.166	0	1	300	5	0.983
307	0.166	0	1	530	34	0.936
310	0.166	0	1	527	6	0.989
314	0.166	0	1	300	1	0.997
349	0.166	0	1	500	12	0.976
280	0.166	0	2	500	29	0.942
313	0.166	0	2	300	0	1.000
350	0.166	0	2	538	5	0.991
288	0.166	0	3	500	16	0.968
310	0.166	0	3	500	8	0.984
353	0.166	0	3	548	3	0.995
308	0.166	0	4	500	5	0.990
306	0.166	0.90	2	300	10	0.967
310	0.166	0.15	2	500	16	0.968
312	0.166	0.32	2	500	37	0.926
347	0.166	0.78	2	536	25	0.953
309	0.166	0.77	4	500	38	0.924
403	0.142	0.50	3	493	5	0.995

Initial attempts to perform similar semi-steady-state tests at temperatures below 200°C yielded significantly lower conversions (below 50%). However, it was discovered that higher levels of NO_x removal could be attained by adsorbing NH_3 at higher temperatures (i.e., above 300°C), while performing NO_x reduction at temperatures as low as 125°C. The possibility of NH_3 adsorption limitations at lower temperatures was discounted by subsequent FTIR experiments which confirm that NH_3 adsorbs strongly on Brønsted acid sites at low temperatures (refer to FTIR results). Table 2 lists results of tests performed in this manner (i.e., NH_3 adsorption carried out between 320 and 350°C) over H-M-5 with NO reduction reactions carried out between 125 and 210°C. At 125°C, NO_x removal efficiencies greater than 30% are observed (2% O_2, GHSV = 24,000), while at 200°C close to 100% NO removal is observed (4% O_2, GHSV = 24,000). These results confirm that elimination of gaseous NH_3 inhibition effects substantially enhances the SCR of NO on H-mordenite at low temperatures. In addition, high-temperature NH_3 adsorption also promotes greater SCR activity possibly by activation of adsorbed NH_3 (see Discussion).

NO removal data listed in Table 2 were linearly regressed to determine the activation energy and form of the overall reaction rate expression. For the data to fit a first order dependency on NO concentration and assuming that the partial pressure of O_2, P_{O_2}, is constant throughout the three reactors, the reaction rate constant, k, must fit the expression (22)

$$W_1P_1 + W_2P_2 + W_3P_3 = \frac{-F_{T_0}}{kP_{O_2}^n}\ln(1 - X), \qquad [2]$$

where W_i is the mass of catalyst in reactor i, P_i is the total

TABLE 2

Semi-Steady-State Kinetics Obtained over H-M-5 with NH_3 Adsorption Performed at $T > 300$°C ($Q = 150$ cm^3/min)

W (g)	T (°C)	[O_2] (%)	[NO] in (ppm)	[NO_x] out (ppm)	NO_x removal
0.279	125	2	478	314	0.343
0.279	130	4	475	309	0.349
0.279	145	2	490	282	0.424
0.279	147	1	494	287	0.419
0.279	147	4	486	267	0.451
0.279	148	3	513	292	0.431
0.279	161	3	504	198	0.607
0.142	163	3	494	214	0.567
0.142	168	4	489	173	0.646
0.142	174	4	489	208	0.575
0.279	175	2	490	95	0.806
0.279	177	3	483	71	0.853
0.279	179	1	550	194	0.647
0.142	179	2	500	225	0.550
0.279	182	4	485	40	0.918
0.142	185	3	497	109	0.781
0.142	188	4	491	70	0.857
0.142	193	4	493	55	0.888
0.142	198	3	493	84	0.830
0.279	198	4	488	1	0.998

pressure in reactor i, F_{T_0} is the total inlet molar flow, X is the overall NO conversion through all three reactors, and n is the reaction rate order for O_2.

Regression of the data yields a reaction rate order for O_2 of 0.24 ± 0.02 and an activation energy of 56.4 ± 1.1 kJ/mol (Fig. 5), which agrees well with values of 60.6 kJ/mol reported in our previous study (21) for H-ZSM-5 (330°C $> T >$ 430°C), 54.0 kJ/mol reported by Nam *et al.* (23) for H-mordenite (225°C $> T >$ 500°C) and 58 kJ/mol reported by Andersson *et al.* (14) for a commercial H-mordenite catalyst (Zeolon 900 H tested at 227°C $> T >$ 327°C). It should be noted, however, that the data in Fig. 5, which are based upon NO removal, actually encompass several different rates: (i) the rate limiting step in NO reduction by adsorbed NH_3 in the presence of O_2, (ii) adsorption of NO_x species, and (iii) activation of adsorbed NH_3 species.

Addition of low concentrations of H_2O (<1%) at high temperatures resulted in only minor decreases in the amounts of NO_x removed in semi-steady-state kinetic tests (Table 1). This observation is consistent with results of steady-state kinetic tests performed in our previous study (21). However, inhibition by H_2O was observed during low-temperature tests ($T <$ 200°C). Although tests were not continued to steady state, it was observed that at temperatures below 200°C, H_2O addition resulted in monotonic increases in effluent NO_x concentrations with time. These qualitative results reflect the competitive adsorption of H_2O at low temperature since only an inhibition effect is observed when H_2O is added and not permanent catalyst deactivation. Indeed, Bagnasco (24) reported that H_2O displaces weakly adsorbed NH_3 (NH_3 coordinated to aluminum species or adsorbed by hydrogen bridging bonds). The presence of H_2O may also interfere with the NH_3 migration necessary for the formation of active complexes resulting in the inhibition effect observed.

In situ FTIR tests. FTIR tests were initiated by heating pressed wafers of zeolite at 3°C/min to the desired reaction temperature while purging in 100 cm^3/min He. Background spectra were obtained prior to NH_3 adsorption. *In situ* FTIR spectra were recorded at various times during NH_3 adsorption and subsequent reaction of adsorbed NH_3 with NO_x and O_2. An initial FTIR test was performed over H-M-5 at 470°C in an attempt to identify possible intermediate species. Adsorption of NH_3 was performed until no visible change in the magnitude of the adsorption bands was detected. The wafer was then flushed with He and then switched over to a stream containing 1500 ppm NO and 2.2% O_2. Spectra were obtained 2, 6, 7, and 8 min after the switch-over (Fig. 6). Large peaks at 1450 and 3245 cm^{-1},

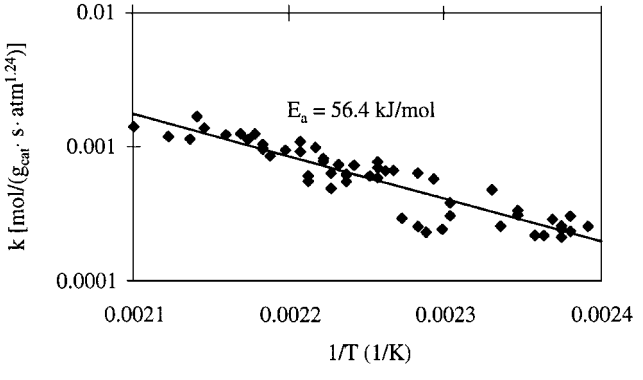

FIG. 5. Arrhenius plot of reaction rate constants for SCR on ammonia-pretreated (preadsorbed at 320–350°C) H-M-5 obtained in semi-steady-state reaction tests with a feed containing 500 ppm NO and 1–4% O_2.

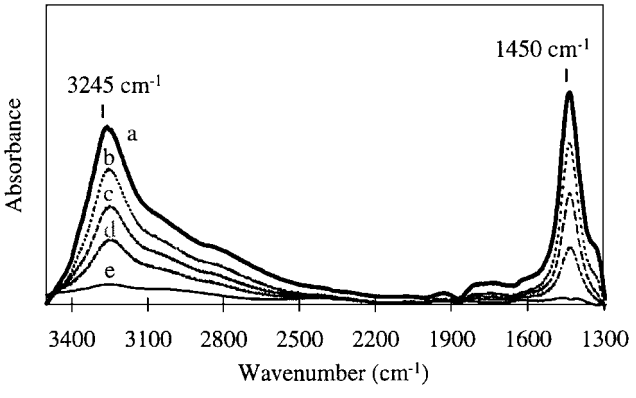

FIG. 6. Transient FTIR spectra obtained while passing 1500 ppm NO and 2.2% O_2 at 471°C over H-M-5 containing NH_3 preadsorbed at 471°C: (a) initial, (b) 2 min, (c) 6 min, (d) 7 min, and (e) 8 min.

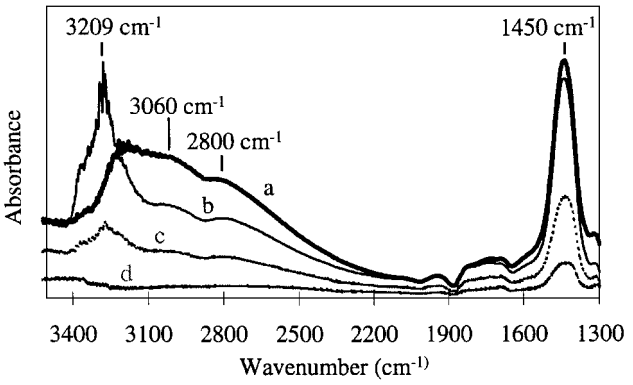

FIG. 7. Transient FTIR spectra obtained while passing 1500 ppm NO and 2.2% O_2 at 300°C over H-Z-12 containing NH_3 preadsorbed at 300°C: (a) 2 min, (b) 3 min, (c) 8 min, and (d) 10 min.

which correspond to NH deformation vibrations (25) and NH stretching frequencies of NH_4^+, respectively, are observed to decrease as a function of time. These spectra confirm that adsorbed NH_3 reacts with NO and O_2. Additional minor bands (also associated with NH stretches) are observed at approximately 2800 and 3060 cm^{-1}. Noticeably absent is the appearance of any bands associated with adsorbed NO_x species (primarily observed at wavenumbers between 1500 and 2000 cm^{-1}). This is presumably due to the low concentrations of adsorbed NO_x intermediates at high reaction temperatures.

A similar test performed with H-Z-12 at 300°C resulted in the spectra shown in Fig. 7. Even at this lower temperature, NO_x intermediate species are not detected. Interesting trends are observed, however, in the magnitude of bands associated with NH stretches. The spectra obtained 2 min after injection of 1500 ppm NO and 2.2% O_2 show dominant NH stretches at wavenumbers of approximately 2800 and 3060 cm^{-1}. Within the next minute, a reconfiguration occurs which results in a larger concentration of NH_4^+ molecules with a dominant NH stretch at 3209 cm^{-1}.

Teunissen and co-workers (26) performed *ab initio* quantum chemical cluster calculations to determine the nature of NH_4^+ cation coordination in zeolites. Their results indicate that the most energetically favorable coordinations of NH_4^+ cations to the zeolitic cluster are with two or three hydrogen bonds (referred to as 2H and 3H, respectively). Moreover, the NH stretching region of the FTIR spectra of NH_4^+-zeolites can be explained as a superposition of the spectra of the 2H and 3H structures. As shown in Fig. 8, the frequencies for the 2H structure in mordenite are approximately 2800 and 3040 cm^{-1}, while the dominant frequency for the 3H structure is 3270 cm^{-1} (a small shoulder at 3360 cm^{-1} corresponds to the stretch of the proton pointing away from the zeolitic cluster). Based upon these explanations of NH_4^+ cation coordination, Fig. 7 suggests that a rearrangement of NH_4^+ molecules from the 2H to the 3H structure occurs before significant reaction occurs. Thus, the 3H structure appears to be the coordination which is most favorable for reaction with NO_x to form N_2. This is consistent with Fig. 6, which shows that the 3H structure is more prevalent at 470°C. Furthermore, a comparison of the FTIR spectra of NH_3 adsorbed on H-Z-26 at 22, 178, and 327°C (Fig. 9) indicates that the 2H structure is more stable at lower temperatures, while the 3H structure is favored at higher temperatures. Thus, the increased activity at higher temperatures may be partially attributed

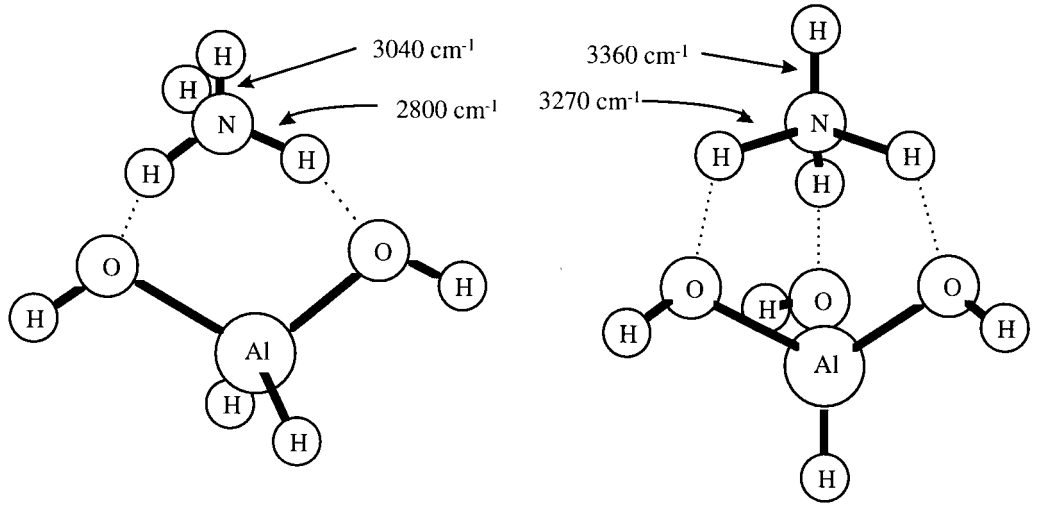

FIG. 8. 2H and 3H structures of NH_4^+ bonded to zeolite clusters (Teunissen *et al.*, 1993).

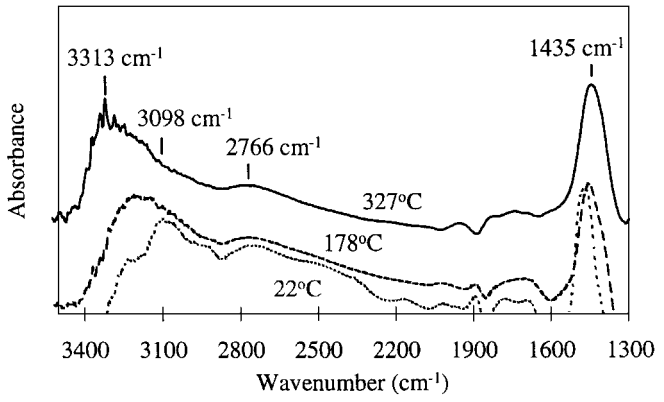

FIG. 9. Comparison of FTIR spectra showing bands for NH_3 adsorption on H-Z-26 at different temperatures.

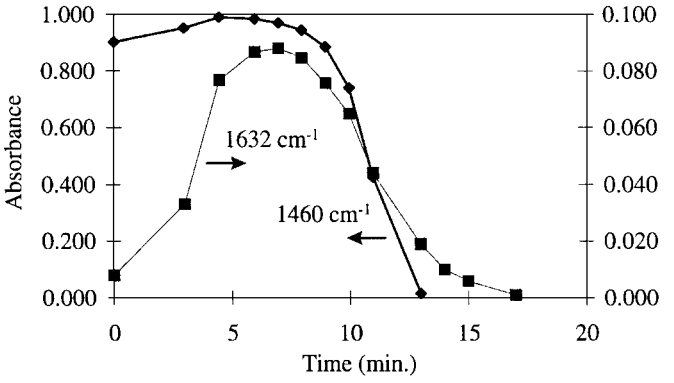

FIG. 11. Changes in absorbances at 1460 and 1632 cm^{-1} with time observed while passing 3000 ppm NO and 4.4% O_2 at 195°C over H-Z-12 containing NH_3 preadsorbed at 330°C.

to the preferable NH_4^+ cation configuration at higher temperatures.

In view of the apparent higher reactivity of the 3H structure of adsorbed NH_3 and the enhanced stability of this structure over the 2H configuration at higher temperatures, a separate set of *in situ* FTIR tests was performed to identify the NO_x intermediate in the SCR of NO. In these tests, NH_3 was adsorbed onto a zeolite wafer at approximately 330°C until the FTIR spectrum showed no indication of further NH_3 adsorption. The wafer was then purged with He and cooled to below 200°C at 3°C/min (total purging time typically exceeded 1 h). NO and O_2 were then passed over the wafer and *in situ* FTIR spectra were recorded at regular intervals thereafter. Figure 10 displays selected FTIR spectra obtained after passing 3000 ppm NO and 4.4% O_2 over an H-Z-12 sample at 195°C. Of particular interest is the transient behavior of a small band at 1632 cm^{-1} which is not present initially, but which appears with increasing intensity shortly after introduction of NO and O_2. As adsorbed NH_3 diminishes due to reaction, the band disappears. These trends are more easily distinguished in Fig. 11, which displays the transient nature of the band at 1632 cm^{-1} in comparison with the band at 1460 cm^{-1} (the NH_4^+ deformation band was observed to shift between values of 1443 and 1460 cm^{-1}). From this figure, it is apparent that NH_3 does not react (as indicated by a decrease in the NH_4^+ deformation band) until an intermediate species with a stretching frequency at 1632 cm^{-1} is formed. As adsorbed NH_3 disappears by reaction, the intermediate species concentration also decreases.

A temperature-programmed reaction test performed with H-M-5 confirms that the same intermediate species appears when reactions are carried out over mordenite catalysts. For this test, an H-M-5 wafer was presorbed with NH_3 at 340°C, flushed with He, and then cooled to 100°C. Baseline spectra were collected at this point, after which a He stream containing 1500 ppm NO and 2.2% O_2 was introduced. Figure 12 shows selected FTIR spectra obtained as the temperature is ramped from 100°C at 3°C/min. The appearance of a band at 1632 cm^{-1} is readily observed. When this band reaches a maximum value (after approximately

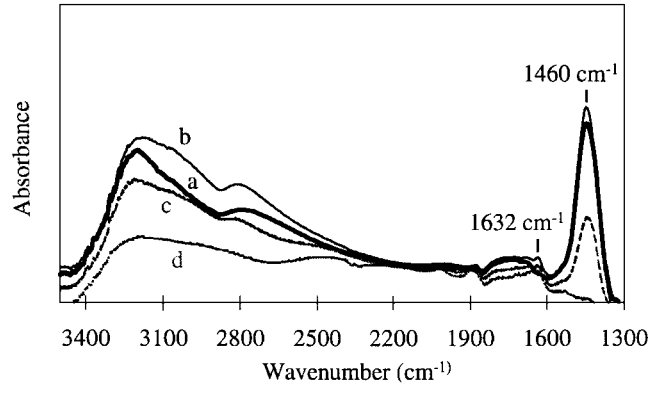

FIG. 10. Transient FTIR spectra obtained while passing 3000 ppm NO and 4.4% O_2 at 195°C over H-Z-12 containing NH_3 preadsorbed at 330°C: (a) initial, (b) 6 min, (c) 11 min, and (d) 13 min.

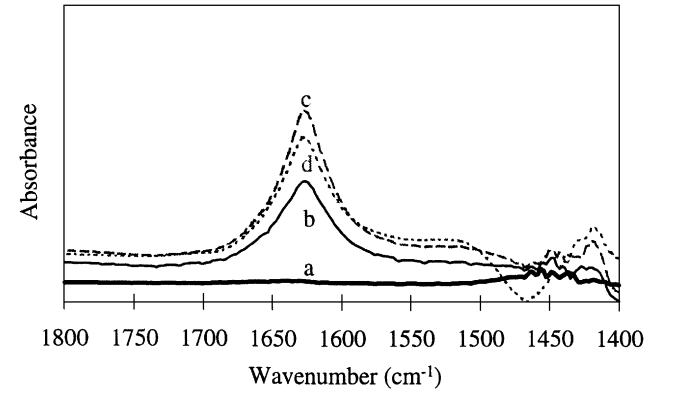

FIG. 12. Transient temperature-programmed FTIR spectra obtained while passing 1500 ppm NO and 2.2% O_2 at 195°C over H-M-5 containing NH_3 preadsorbed at 340°C; temperature ramp of 3°C/min from (a) 100°C (initial), (b) 120°C (7 min), (c) 141°C (14 min), and (d) 160°C (20 min).

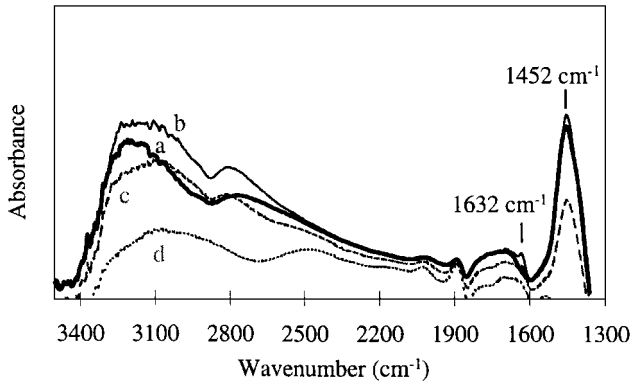

FIG. 13. Transient FTIR spectra obtained while passing 3000 ppm NO and 4.4% O_2 at 178°C over H-Z-26 containing NH_3 preadsorbed at 325°C: (a) initial, (b) 6 min, (c) 9 min, and (d) 13 min.

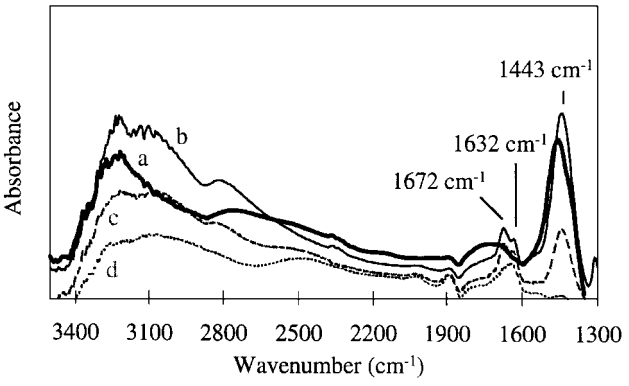

FIG. 15. Transient FTIR spectra obtained while passing 4820 ppm NO_2 (no oxygen) at 178°C over H-Z-26 containing NH_3 preadsorbed at 325°C: (a) initial, (b) 5 min, (c) 10 min, and (d) 14 min.

14 min of reaction time or at 141°C), the band at 1460 cm^{-1} (NH_4^+ deformation band) begins to decrease. As the NH_3 continues to react away, the band at 1632 cm^{-1} also begins to decrease. The similarity in species concentration trends between reactions over H-ZSM-5 and H-mordenite suggests that the same intermediate species and reaction steps are involved in SCR with both zeolites.

To examine the influence of acid site concentration, *in situ* FTIR tests were also performed with H-Z-26. After NH_3 adsorption and He purging at 325°C, the wafer was cooled to 178°C. Figure 13 shows the transient *in situ* FTIR spectra obtained 6, 9, and 13 min after a stream containing 3000 ppm NO and 4.4% O_2 in He was exposed to the zeolite wafer. Comparison of the absorbances at 1632 and 1452 cm^{-1} (Fig. 14) reveals the same correlation between the presence of the intermediate NO_x species and reactivity of adsorbed NH_3. Disappearance of the band at 1632 cm^{-1} as NH_3 reacts also suggests that the intermediate species complexes with NH_4^+ and does not merely adsorb onto adjacent sites. It is also interesting to note that there is a slight increase in NH_4^+ concentration (as given by the magnitude of the band at 1452 cm^{-1}) as the NO_x intermediate species forms (compare Figs. 11 and 14). This suggests that (i) there is additional NH_3 present which is not adsorbed onto Brønsted acid sites even though samples are typically purged in He for over 1 h after NH_3 adsorption, (ii) there are free Brønsted acid sites that do not form NH_4^+ complexes after adsorption and subsequent purging, and (iii) the NO_x intermediate species promote adsorption of excess NH_3 onto free Brønsted acid sites. The first two points are in agreement with results observed in the modified steady-state tests, while the third point helps to explain the activation phenomenon observed in the transient tests explained earlier in this study.

The initial increase in NH_4^+ ion concentration after addition of NO_x is more pronounced when reducing NO_2 (with or without O_2). Figure 15 displays the FTIR spectra obtained 5, 10, and 14 min after flowing 4820 ppm NO_2 in He at 178°C over the same H-Z-26 wafer (NH_3 presorption carried out in the same manner as mentioned previously). As NO_2 is introduced, bands associated with the 2H and

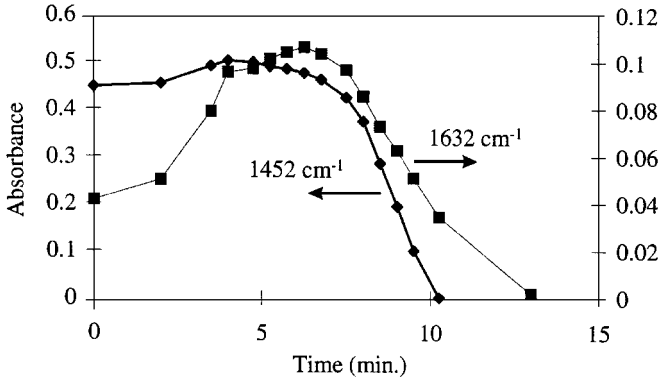

FIG. 14. Changes in absorbances at 1452 and 1632 cm^{-1} with time observed while passing 3000 ppm NO and 4.4% O_2 at 178°C over H-Z-26 containing NH_3 preadsorbed at 325°C.

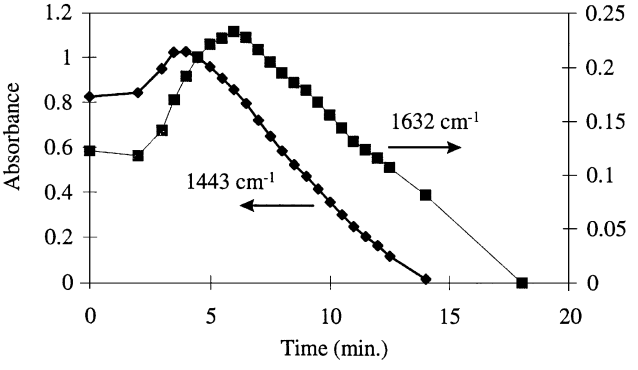

FIG. 16. Changes in absorbances at 1443 and 1632 cm^{-1} with time observed while passing 4820 ppm NO_2 (no oxygen) at 178°C over H-Z-26 containing NH_3 preadsorbed at 325°C.

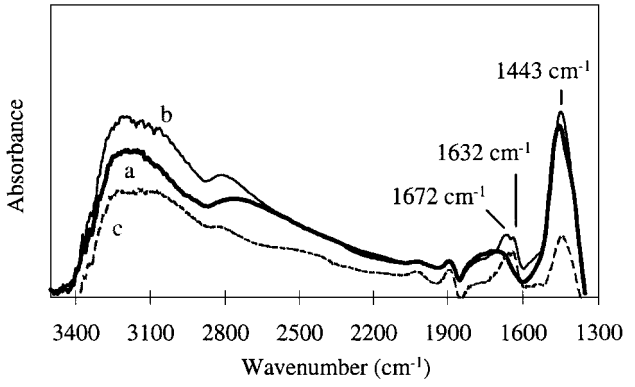

FIG. 17. Transient FTIR spectra obtained while passing 3000 ppm NO_2 and 4.4% O_2 at 178°C over H-Z-26 containing NH_3 preadsorbed at 325°C: (a) initial, (b) 4 min, and (c) 13 min.

3H structures (at 2802 and 3064 cm^{-1}, and 3209 cm^{-1}) increase and consequently the total NH_4^+ ion concentration increases. Figure 16 more clearly illustrates the increase in NH_4^+ concentration as reaction proceeds by comparing the absorbances at 1443 and 1632 cm^{-1}. The observation that only NO_2 (without O_2) causes increases in the bands at 1443 and 1632 cm^{-1} supports the hypothesis that NO_2 is an active intermediate in the SCR reaction (i.e., NO_2 is responsible for the band at 1632 cm^{-1}). However, reactions with NO_2 also result in the formation of another adsorbed species revealed by the band at 1672 cm^{-1}. Even with O_2 added to NO_2, the band at 1672 cm^{-1} still appears (Fig. 17) although it is dampened when O_2 is present.

DISCUSSION

Mechanistic role of adsorbed NH_3. NH_3 has been used widely as a probe molecule for determining acid-site concentrations of zeolites. Using NH_3 desorption, Hidalgo *et al.* (27) determined that Brønsted acid sites account for 60% of the total Al content in mordenite. Crocker *et al.* (28) used NH_3 titration to determine the number of acid sites in H-ZSM-5 and H-mordenite and found that NH_3 adsorbs on 70% of the theoretical maximum number of acid sites. Li and Hall (4) also determined a similar NH_3/Al ratio of 0.77 for H-ZSM-5. In comparison, measurements of N_2 formation during transient tests with H-M-5, H-Z-12, and H-Z-26 (i.e., flowing NO and O_2 over NH_3-presorbed zeolites) reveal ratios of N_2 formed/Al between 0.34 and 0.46. Based upon a stoichiometry of 1.0 NH_3 reacted/N_2 formed (reaction [1]), comparison of the ratios of NH_3 adsorbed/Al ($\sim$0.75) versus N_2 formed/Al (0.34–0.46) indicates that approximately half of the adsorbed NH_3 is active for N_2 formation.

These results can be explained by a mechanism in which either (i) only half of the Brønsted acid sites are active for SCR or (ii) adsorbed NH_3 molecules on pairs of acid sites are involved in the formation of each N_2 molecule. To distinguish between these possibilities, it should be noted that other transient tests, which indicate H-M-10 and H-Z-35 to be inactive, suggest that a threshold Al content exists below which SCR activity is negligible. In addition, Hidalgo *et al.* (27) and Chen *et al.* (29) found that acid sites within H-ZSM-5 have uniform strength. Thus, it is unlikely that only selected isolated acid sites are active for SCR reactions. Conversely, it is possible that for zeolites with high Al concentrations, NH_3 molecules adsorbed onto neighboring acid sites may be close enough to facilitate reaction of pairs of adsorbed NH_3 molecules with gaseous NO_x species (21). Moreover, a mechanism involving paired sites is similar to that suggested by Komatsu *et al.* (10), who proposed that NH_3 adsorbed on pairs of adjacent Cu^{2+} sites are involved in the reduction of NO. Since the activation energy determined for SCR of NO_x by NH_3 over Cu-ZSM-5 (49 to 54 kJ/mol) is similar to that determined in this study for H-M-5 (56.4 kJ/mol) in semi-steady-state tests, it is conceivable that the reaction mechanism is also similar.

In the semi-steady-state tests, the number of moles of NH_3 injected per cycle to maintain constant NO removal was calculated assuming an adsorption ratio of 1.0 NH_3/Al; i.e., the moles of NH_3 injected were equal to the moles of Al in the zeolite sample. From measurements of NH_3 desorption from H-form zeolites in TPD experiments, however, not all Al atoms form Brønsted sites onto which NH_3 adsorbs. Nevertheless, the total amount of NH_3 injected based on this ratio was sufficient to remove an equivalent molar quantity of NO. This suggests that a fraction of the weakly adsorbed NH_3 was not desorbed during purging in the semi-steady-state tests (samples were purged in He for only 15–20 min), but was still present in the pores of the zeolite and could diffuse to and adsorb onto active acid sites vacated as a result of reaction. It is possible that the excess NH_3 resists desorption due to weak association with NH_4^+ ions (26, 30). From stoichiometry, the amount of weakly adsorbed NH_3 is equal to the amount of acid sites upon which NH_3 is not directly adsorbed. Thus, it appears that each Al atom facilitates storage of an NH_3 atom through a combination of direct NH_3 adsorption onto Brønsted acid sites (forming NH_4^+ ions) and weak NH_3 bonding with NH_4^+ ions. Although pairs of acid sites appear to be involved in the reduction of NO atoms, each adsorbed NH_3 atom is capable of reacting or complexing with an NO or NO_2 atom.

FTIR results reveal that specific configurations of NH_4^+ molecules are necessary for high SCR activity. From Fig. 7, which displays the transient FTIR spectra obtained as NO and O_2 react with adsorbed NH_3 on H-Z-12 at 300°C, it is apparent that a shift occurs in the NH stretching bands of NH_4^+. Specifically, before reaction proceeds (as indicated by decreases in magnitude of the NH_4^+ deformation band at 1450 cm^{-1}), a rearrangement occurs resulting in a decrease in the bands at 2800 and 3060 cm^{-1}, accompanied by an increase in the band at 3209 cm^{-1}.

From *ab initio* quantum chemical cluster calculations, Teunissen *et al.* (26) concluded that NH_4^+ cations are most energetically stable when coordinating with a zeolite cluster through two or three hydrogen bonds (2H and 3H structures, respectively). Furthermore, they assigned the bands at 2800 and 3060 cm^{-1} to the 2H configuration, while the band at 3209 cm^{-1} was assigned to the 3H structure. Thus, the transient FTIR spectra indicate that the more active NH_4^+ configuration is the 3H structure and that NO_x interactions with adsorbed NH_3 enhance reconfiguration to this structure.

The same reconfiguration is not observed at higher temperatures (Fig. 6 shows spectra obtained at 471°C) because the 3H structure is already the predominant configuration. This is further evident from comparison of the FTIR spectra of NH_3 adsorbed onto H-Z-26 at 22, 178, and 327°C (Fig. 9) showing that the 3H structure is more prevalent at higher temperatures, while the 2H structure is favored at lower temperatures. Thus, the temperature of NH_3 adsorption is important, not only for increasing reaction rates, but also for facilitating the preferred coordination of NH_4^+ cations. This explains why high-temperature NH_3 adsorption (>325°C) during modified steady state tests results in higher reaction rates. In contrast, semi-steady-state tests carried out by performing both reactions and NH_3 adsorption at temperatures below 200°C result in considerably lower conversions.

Role of acidity and zeolite structure. Brønsted acid sites in zeolites are important as NH_3 adsorption sites. However, our previous work (21) and results of this work provide evidence that SCR activity of H-zeolites is associated with pairs of Brønsted acid sites which are close enough to enable reactions between NO_x and pairs of adsorbed NH_3 molecules. This would explain the inactivity of high Si/Al zeolites, such as H-M-10 and H-Z-35. Acid site concentration, though, is not the only factor affecting the SCR activity of zeolites. Our experimental observations support the argument that zeolite pore structure also plays an important role in influencing the Si/Al ratio at which a particular type of zeolite becomes active. For instance, H-Y-2.5 is catalytically inactive despite its high acid site concentration, while H-M-5 and H-Z-12 are active SCR catalysts.

Y zeolite consists of a three-dimensional network of interconnecting sodalite cages and supercages having diameters of 6.6 and 11.4 Å, respectively. However, molecules preferentially adsorb within large-diameter 7.4-Å channels leading to the larger supercages. Since NH_3 adsorption in Y zeolite is dominated by the 2H configuration (26), it is probable that the large diameter channels and supercages of Y zeolite favor the less-active configuration of adsorbed NH_3.

In contrast to the large-diameter pores and supercages of Y zeolite, mordenite consists of a one-dimensional network of smaller-diameter 6.5- to 7.0-Å channels interconnected by smaller side channels, while ZSM-5 consists of a contorted two-dimensional network of relatively narrow 5.5-Å channels. In both pentasils, large supercages do not exist and acid sites (NH_3 adsorption sites) are distributed in channels with smaller diameters than those present in Y zeolites. In contrast to adsorption in Y zeolite, NH_3 adsorption in H-mordenite and H-ZSM-5 consists of both the 2H and 3H structures (Figs. 6, 7, and 9). It is conceivable that the smaller radius of curvature in the smaller-diameter channels of mordenite and ZSM-5 enhances H-bonding with framework oxygen atoms resulting in higher concentrations of 3H NH_4^+ structures. Adjacently adsorbed NH_3 molecules may also enhance formation of the 3H configuration through repulsive coulombic interactions. Thus, the enhanced formation of the 3H structure by small pore zeolites, which is apparently associated with the formation of an active complex during SCR, may explain the high activity of H-mordenite and H-ZSM-5 as compared with Y zeolite.

Formation and location of active complexes. Analysis of transient tests (Figs. 3 and 4) reveals that maximum NO removal and N_2 formation rates are not realized immediately after exposure of NO and O_2 to NH_3-presorbed mordenite or ZSM-5. Moreover, once maximum rates are attained, they are not maintained throughout the entire period of reaction. These results suggest that active complexes must be formed between adsorbed NH_3, and gaseous NO and O_2. FTIR results also suggest that intermediate NO_x species react with adsorbed NH_3 to form an active complex (see following discussion). Reaction of NO_x with this active complex then appears to result in high rates of N_2 formation.

Transient and FTIR tests provide evidence that active complexes are formed on both mordenite and ZSM-5. Figure 4 shows that the maximum N_2 formation rate per unit mass of catalyst for a given set of flow conditions is approximately the same, regardless of zeolite type (i.e., ZSM-5 or mordenite) or acid site concentration (i.e., Si/Al = 5, 12, or 26). It is tempting to explain this observation with a mechanism in which the rate-limiting step is not a surface reaction under the test conditions used (e.g., gas phase oxidation of NO to NO_2). However, if the rate-limiting step is a gas-phase reaction, one would anticipate a constant N_2 formation rate for constant reactant concentrations. Due to the nonuniform shape of the N_2 concentration profiles, it is unlikely that a gas-phase reaction is the rate-limiting step. Furthermore, the evidence suggesting involvement of an active complex is more consistent with a surface reaction as the rate-limiting step.

Since our results suggest that N_2 formation originates from reactions between NO_x and active complexes (i.e., surface reactions), a second explanation for the observation that maximum N_2 formation is independent of zeolite type is that the concentrations of reactant species in the rate-limiting step are the same for all three zeolites. In

a mechanism where gas-phase NO_x reacts with an active complex in a zeolite (see following discussion of reaction mechanism), the reactant species include gas-phase NO_x and the active complex in the zeolite. Since inlet gas-phase NO concentrations were the same in each of the tests involving H-M-5, H-Z-12, and H-Z-26 (Fig. 4), on the basis of this explanation, one would expect the number of active complexes per mass of catalyst to be the same for all three zeolites. However, this expectation is apparently contradicted by the fact that H-M-5, H-Z-12, and H-Z-26 have vastly different acid site concentrations. One hypothesis which reconciles this apparent contradiction is that N_2 formation is due primarily to reactions with active complexes located just inside pores near crystallite surfaces. SEM micrographs (Fig. 2) indicate that external crystallite surface areas are similar for H-M-5, H-Z-12, and H-Z-26 (all have crystallite diameters of approximately 1 μm). Thus, the number of active complexes per mass of catalyst could be the same for all three zeolites if complexes form at pore openings near crystallite surfaces. In view of potential restrictions to diffusion through small diameter pores in zeolites (i.e., the energy barrier associated with the diffusion of molecules past strongly adsorbed NH_3 molecules in 5.5- or 7-Å channels is extremely high), it is conceivable that N_2 formation occurs mainly in pore mouths near crystallite surfaces. In other words, the small diameter channels present in mordenite and ZSM-5 appear to be necessary for stabilization of the 3H NH_4^+ structure (as discussed previously); however, these same narrow pore channels may present diffusional hindrances such that the fastest rates of reaction are achieved at pore openings near crystallite surfaces where significant diffusion of reactant NO_x molecules into 5- to 7-Å pores is unnecessary. As adsorbed NH_3 molecules near pore entrances are consumed by reaction they can be replaced by adsorbed NH_3 molecules further inside the pores explaining why additional NH_3 adsorption capacity can extend the time of reaction but not the maximum rate (see Fig. 4). High rates of N_2 formation associated with external crystallite surface complexes may also explain why wet-impregnated and ion-exchanged Ga-H-ZSM-5 catalysts exhibit the same SCR activity in NO reduction with methane (4). Although the circumstantial evidence provided above supports the hypothesis that active complexes form at crystallite surfaces, more definitive experiments, using zeolites of differing crystallite sizes, are necessary to provide confirmation.

NO_x intermediates and structure of active intermediate. Although *in situ* FTIR spectra obtained during high temperature reactions (>300°C) do not provide evidence of intermediate NO_x species (Figs. 6 and 7), low-temperature tests (<200°C) are useful in identifying adsorbed NO_x species formed during reaction of NO, O_2 and presorbed NH_3. Figures 10 and 13 reveal the formation of a NO_x species in H-ZSM-5 (in H-Z-12 and H-Z-26, respectively) at 1632 cm^{-1}. Similarly, Fig. 12 shows that a species is also formed at 1632 cm^{-1} in H-M-5; thus, the same intermediate NO_x species is involved in SCR with mordenite and ZSM-5.

Several workers have performed *in situ* FTIR tests to identify adsorbed NO_x species in metal-exchanged zeolite systems; however, results of their studies seldom focused on bands in the 1600–1700 cm^{-1} range. Consequently, only suggestions were provided as to the nature of species assigned to bands in this range. Valyon and Hall (31) performed a study of surface species formed during NO adsorption on Cu-ZSM-5. They assigned bands between 1535 and 1630 cm^{-1} to NO_2-containing species, most likely nitrito (O-bound NO_2) or nitrato (NO_3) species as suggested by Nakamoto (32), but also noted that dimeric NO–NO_2 species may also produce these bands. Aylor *et al.* (33), in studies with Co-ZSM-5, suggested similar species assigning a band at 1633 cm^{-1} to nitrito or nitrate (NO_3^-) species. In a previous FTIR study investigating NO decomposition over Cu-ZSM-5, Aylor *et al.* (34) concluded that 1633 cm^{-1} is best assigned to a bidentate chelating nitrato group and a band at 1673 cm^{-1} is due to weakly adsorbed NO_2. Li and Armor (20) performed diffuse-reflectance FTIR studies of adsorbed NO_x species on Co-ferrierite and suggested that bands at 1627, 1595, and 1540 cm^{-1} correspond to nitro (N-bound NO_2), nitrito, and nitrato species, respectively. Adelman *et al.* (18), in studies of NO adsorption on Cu-ZSM-5, also agreed with the assignment that a band at 1628 cm^{-1} is a nitro group associated with a Cu^{2+} ion. Cheung *et al.* (19) and Hoost *et al.* (35), who both performed FTIR studies with Cu-ZSM-5, assigned bands between 1600 and 1630 cm^{-1} to ON–Cu^{2+}–NO_2^- and NO_2^- species, respectively.

Although there is disagreement regarding the exact nature of the species assigned to the band at 1632 cm^{-1}, there is consensus that it is associated with an NO_2-derived species. This is consistent with an NO_2 reaction intermediate mechanism and discounts the suggestion of nitrosonium ions (Cheung *et al.* (19) assigned a band at 1905 cm^{-1} to NO^+) as active intermediates. From tests performed in our laboratory in which only NO_2 is reacted with adsorbed NH_3, it is evident that NO_2 (with or without O_2) is capable of producing this intermediate. This is in contrast to tests performed with only NO or O_2 alone, in which cases the band at 1632 cm^{-1} does not appear. Therefore, the most plausible intermediate is either a nitro or a nitrito species, since O_2 is not necessary to oxidize NO_2 to nitrate or nitrato species.

Analysis of the trends shown in Figs. 11 and 14 indicates that the NO_x intermediate species is also associated with NH_4^+ ions (1460 cm^{-1}) since the magnitude of the band at 1632 cm^{-1} decreases as adsorbed NH_3 disappears. In order to understand how the NO_x intermediate species is

associated with NH_4^+ ions, it is helpful to review suggestions of other intermediate complexes proposed for NO reduction by NH_3 over zeolites.

Williamson and Lunsford (36), in their study of the mechanism of NO reduction by NH_3 over Cu-Y zeolites, found that Cu^{2+} NH_3 adsorption sites are bonded to an oxide of nitrogen in an active complex. They proposed the following arrangement for the active complex:

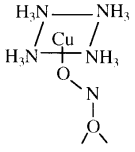

Komatsu *et al.* (10) suggested that the rate-limiting step in SCR with NH_3 over Cu-ZSM-5 involves reaction between a molecule of NO and a dissociated O_2 molecule (or NO_2) with a bridging oxygen atom:

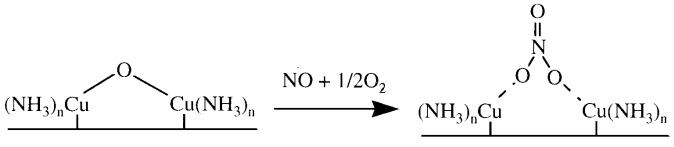

[3]

By analogy, we believe it is possible that the intermediate NO_x species observed at 1632 cm^{-1} is also a nitrito group with oxygen atom(s) of NO_2 interacting with two adsorbed NH_3 molecules. Since experimental results suggest that two NH_3 molecules adsorbed onto neighboring acid sites in the 3H configuration are involved in the reaction, the steps leading to formation of the active complex would probably consist of reactions [4] and [5]:

$$NO + \frac{1}{2}O_2 \leftrightarrow NO_2 \qquad [4]$$

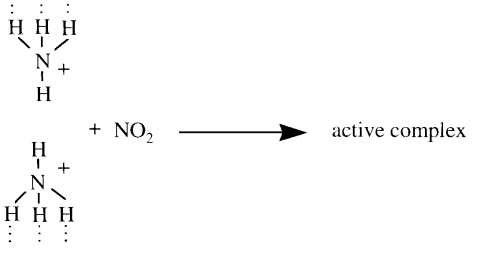

[5]

While the active complex is shown to be formed by reaction between two neighboring NH_4^+ ions and an NO_2 molecule, the precise nature of the active complex is not clear. Valyon and Hall (31) suggested that extralattice oxygen atoms in Cu-ZSM-5 may be adsorption sites for NO molecules, but were unclear about the nature of these sites. It is also possible, however, that the nitrito group observed in the FTIR spectra of this study is not bound to the zeolite, but interacts with the neighboring NH_4^+ groups. Thus, two possible configurations of the active complex are as follows:

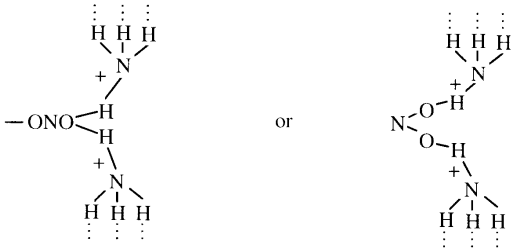

Complex A Complex B

In Complex A, a nitrito group is shown bound to the zeolite while the NH_4^+ ions act as electron sinks causing association between the nitrito group and the adsorbed NH_3. Complex B shows a second alternative in which a nitrito group is not bound to the zeolite, but forms a bidentate bond to two NH_4^+ groups. In each case, interactions between the NO_2 molecule and the free hydrogen atoms of NH_4^+ ions expose the nitrogen atoms of NH_3 to facilitate further interactions with NO_x.

SCR mechanism. As illustrated in reaction [5] above, NO_2 is proposed to be an important intermediate/reactant in the SCR of NO_x over H-form zeolites. However, Brandin *et al.* (15) noted that maximum NO_x reduction is achieved when ratios of $NO_2 : NO_x$ of 1 : 2 are present in the reactant mixture. Since maximum NO_x reduction is not achieved at 1 : 1 ratios of NO_2/NO_x, NO must also function as a reactant in N_2 formation, i.e., is not only a reactant in the formation of NO_2. In view of this observation, the step leading to N_2 formation (since no N_2O has been observed in NO reduction) is proposed to be a reaction between NO and the active complex as shown in reaction [6] (Complex B has been used to represent the active complex for presentation purposes):

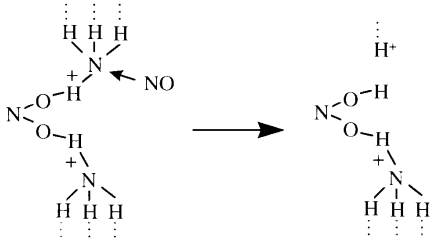

[6]

Although reaction [6] is illustrated as a single step, the influence of hydrogen bonding and hydrogen rearrangement (in view of the large number of hydrogen atoms in the active complex) may play an important role in causing dissociation of the NO molecule. It is possible that the reaction of NO with the nitrogen of adsorbed NH_3, as shown above, may proceed in a manner similar to the high-temperature, gas-phase reaction of NO with amidogen radicals (NH_2). In the gas-phase reaction (thermal $DeNO_x$), a weak bond between the nitrogen atoms of NO and NH_2 develops (Fig. 18).

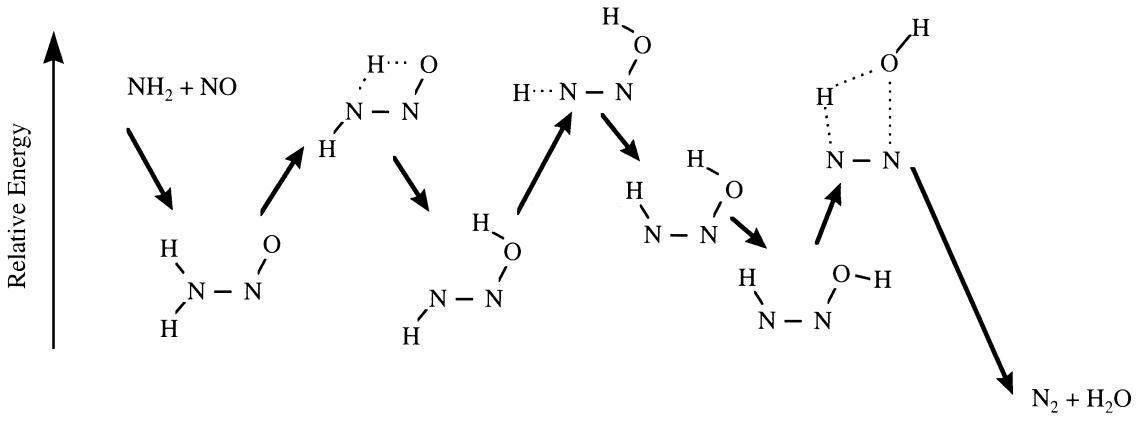

FIG. 18. Structures of N_2H_2O intermediates and transition states in thermal $DeNO_x$ (37).

As the amidogen hydrogen atoms rearrange to associate with the oxygen atom of NO, the N–O bond weakens and the N–N bond strengthens, resulting in the formation of N_2 and H_2O molecules (37). Similarly, the influence of hydrogen bonding may be important in zeolite-catalyzed SCR in view of documented activation of molecular hydrogen to form protonic acid sites in zeolites (38). As a result of reaction [6], a catalytic Brønsted acid site is restored and an undissociated complex remains. This complex may further dissociate to form additional N_2 and H_2O and restore a second Brønsted acid site:

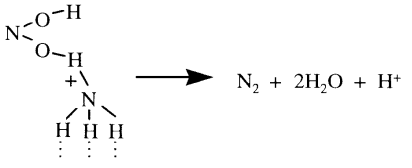

[7]

Again dissociation of the residual complex is shown as a single step; however, it likely involves significant rearrangement before the decomposition products are produced. Since no evidence is available regarding the association of hydrogen atoms during SCR reactions, the assignment of hydrogen bonds in reactions [6] and [7] is somewhat arbitrary. It is possible that hydrogen atom migration within a zeolite may also be involved in the SCR reaction steps. The net result of the steps shown in reactions [4]–[7] is

$$2H^+ + 2NH_3 + NO + 0.5O_2 + NO \rightarrow 2N_2 + 3H_2O + 2H^+. \quad [8]$$

This is the same stoichiometry given by reaction [1].

While this mechanism has been developed to describe NO reduction over H-form zeolites, it can also be adapted to account for NO_2 reduction. Reaction [5] remains unaltered; however, no NO is available in reaction [6] to react with the active complex. With only NO_2 available for reaction, the limited quantity of hydrogen atoms (disregarding hydrogen mobility effects) suggests that insufficient hydrogen is available to abstract both of the oxygen atoms from NO_2 resulting in the formation of stoichiometric levels of N_2O as shown in reaction [9]:

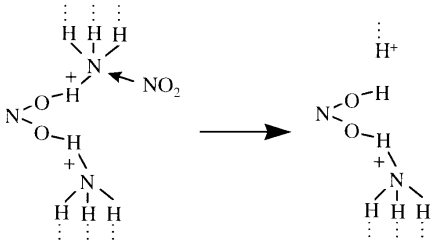

[9]

Dissociation of the residual complex would proceed in the same manner as shown in reaction [7], leading to the following stoichiometry for NO_2 reduction (without O_2):

$$2H^+ + 2NH_3 + 2NO_2 \rightarrow N_2 + N_2O + 3H_2O + 2H^+. \quad [10]$$

Reaction [10] predicts equimolar formation of N_2 and N_2O. This stoichiometry is consistent with results of an isotopic labeling study in which $^{14}NO_2$ was reacted with presorbed $^{15}NH_3$ over H-M-5 (22). Analysis of the mechanism also indicates that a nitrogen atom from NH_3 reacts with a nitrogen atom from NO_2 to form each of the N_2 and N_2O molecules. These mechanistic predictions are also consistent with results of the aforementioned isotopic labeling study. Product concentrations measured in the isotopic labeling study revealed virtually equimolar formation rates of $^{14}N^{15}N$ and $^{14}N^{15}NO$ after an initial transient period (i.e., a nitrogen atom from NH_3 reacts with a nitrogen atom from NO_2 to form each of the N_2 and N_2O molecules). No evidence of any other N_2O isotope was detected and only trace amounts of $^{14}N_2$ were measured which were attributed to impurities. Thus, isotopic labeling studies also support the proposed mechanism.

A catalytic cycle illustrating the proposed mechanism for SCR of NO_x with NH_3 is illustrated in Fig. 19. The initial step

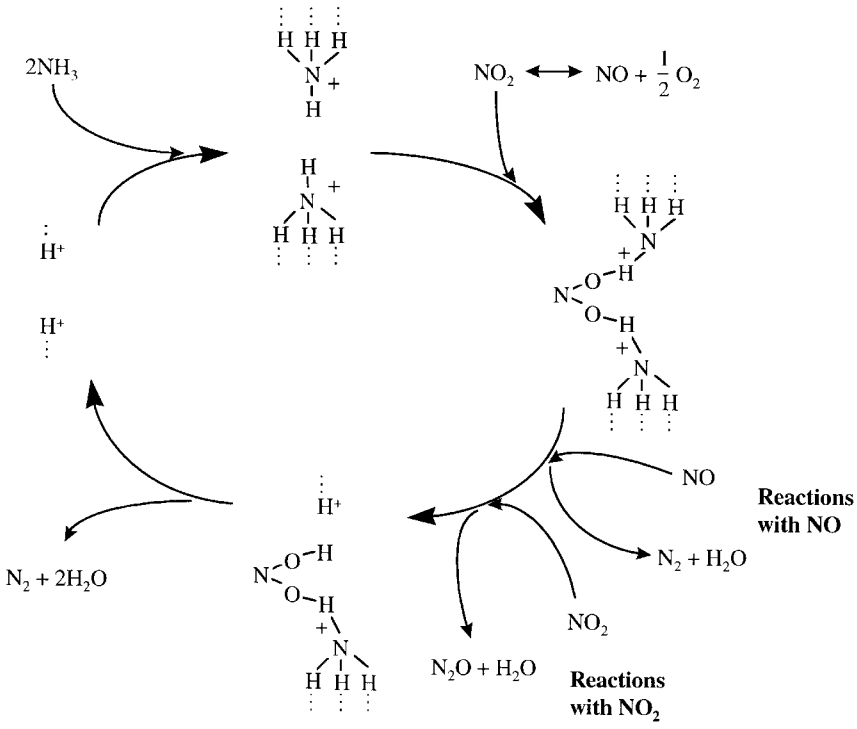

FIG. 19. Reaction mechanism of SCR of NO_x with NH_3 over H-form zeolites.

in this mechanism is the adsorption of NH_3 onto neighboring acid sites; however, this could also include rearrangement of the NH_4^+ complexes to the 3H structure. The next step involves reaction of adsorbed NH_3 with NO_2 to form an active complex. This step, which may include NO oxidation to NO_2 or diffusion of NO_2 to adsorbed NH_3 if significant gas-phase NH_3 is present, is the rate-limiting step in the initial formation of N_2. Once the active complex is formed, it reacts rapidly with NO or NO_2 to form N_2 or N_2O, respectively. The residual complex is shown to decompose to N_2 and H_2O; however, it is probable that this reaction involves several rearrangement steps which may be slow. It is also possible that the decomposition process is enhanced by interactions with other NH_3 molecules or mobile hydrogen atoms.

The overall mechanism shown in Fig. 19 explains several experimental observations: (i) the reactant stoichiometry observed in SCR (i.e., $NO : NH_3 : O_2 = 4 : 4 : 1$), (ii) the absence of N_2O formation during NO reduction, (iii) the formation of N_2O during NO_2 reduction, and (iv) the enhancement in activity when 1 : 1 NO/NO_2 ratios are used.

Aspects of the mechanism shown in Fig. 19 may also explain the importance of zeolites in SCR. The initial step in SCR by NH_3 over H-mordenite or H-ZSM-5, as shown in Fig. 19, is the adsorption and stabilization of NH_3 onto Brønsted acid sites in the 3H configuration. While the importance of this adsorption configuration has previously been discussed in explaining the inactivity of Y zeolites, similar adsorption and stabilization of other hydrogen-containing reactive intermediates may be important in SCR with hydrocarbons. Cowan *et al.* (9), for instance, proposed that the rate-limiting step in SCR of NO by CH_4 over Co-ZSM-5 is the abstraction of a hydrogen atom from CH_4 to form a methyl species. This methyl species was then proposed to be the intermediate species responsible for NO reduction to N_2 and it is possible that the zeolite is necessary to stabilize this reactive intermediate. Lercher *et al.* (39) proposed that a carbocation in a zeolite is a "transition state stabilized by nearly covalent interactions of two of its protons with two negatively charged oxygens in the vicinity of the aluminum atom." Thus, the zeolite may serve to stabilize hydrogen-containing intermediates (NH_4^+ ions, methyl radicals or carbocations) until reactions with NO_x can occur.

The formation of an active complex of NH_4^+ and an NO_2 intermediate may also help to explain the promoting effect of metal-cation exchange in zeolites. The mechanism shown in Fig. 19 suggests that NO_2 is necessary for the formation of active complexes. However, metal-free zeolites do not facilitate significant storage of NO_x at temperatures above 200°C (2). If excess gaseous NH_3 inhibits NO_x diffusion to acid sites (or adsorbed NH_3) in zeolites (21) and H-form zeolites are not capable of storing NO_2 at temperatures above 200°C, low SCR activities would be expected when injecting NH_3 into NO_x-laden streams over H-form zeolites at temperatures just above 200°C. These low SCR activities are indeed observed at temperatures below 300°C;

however, when excess gaseous NH_3 is removed (i.e., using the NH_3-presorption approach), significant SCR activity is observed at these same temperatures presumably due to elimination of the NH_3 inhibition effect. It is also possible to obtain high NO_x conversions at low temperatures in the presence of excess NH_3 when metal-exchanged zeolites are used. Brandin *et al.* (15), Choi *et al.* (40), and Ham *et al.* (41) all documented high conversions (>90%) of NO at temperatures above 230°C when performing SCR by NH_3 over Cu-mordenite. It is possible that the role of Cu cations is to increase the surface concentrations of NO_2. Indeed, Adelman *et al.* (18) have shown that NO_2-type species are stabilized on Cu-ZSM-5 at temperatures as high as 400°C.

CONCLUSIONS

1. Removal of gaseous NH_3 significantly enhances catalytic activity in the SCR of NO_x with NH_3 over H-form zeolites. Transient and semi-steady-state tests performed using NH_3 presorption verify that NO_x reduction can be carried out at high conversions at temperatures as low as 125°C.

2. Analysis of the transient and semi-steady-state tests suggests that NH_3 adsorbed onto neighboring acid sites is necessary for SCR activity. Furthermore, FTIR results indicate that NH_3 must be adsorbed in a 3H structure (i.e., bonded to the zeolite through three hydrogen bonds) in order to be reactive for SCR. This preferred configuration, which is favored in mordenite and ZSM-5 and less favorable in Y zeolite, may be an indication of the importance of zeolite structure on SCR activity.

3. *In situ* FTIR experiments performed at temperatures below 200°C reveal the appearance of an NO_2-type intermediate in SCR on both H-ZSM-5 and H-mordenite. A mechanism involving NO_2 interaction with pairs of adsorbed NH_3 resulting in the formation of an active complex which then reacts with NO to form N_2 is most consistent with experimental observations.

4. The initial step in the proposed reaction mechanism is adsorption of NH_3 onto neighboring acid sites and rearrangement of the NH_4^+ complexes to the 3H structure. The next step involves reaction of adsorbed NH_3 with NO_2 to form an active complex. This active complex reacts rapidly with NO or NO_2 to form N_2 or N_2O, respectively, leaving a residual complex. The residual complex then decomposes to form additional N_2 and H_2O.

5. The proposed reaction mechanism explains the following experimental observations: (i) 1 : 1 NO_2 : NO ratios are optimal for maximum NO_x conversion to N_2, (ii) reactant stoichiometries for NO reduction by NH_3 are $4NO : 4NH_3 : 1O_2$, (iii) the only nitrogen-containing species formed during NO reduction in the presence of O_2 is N_2, and (iv) NO_2 reduction results in the formation of 50% N_2 and 50% N_2O.

ACKNOWLEDGMENTS

We gratefully acknowledge the assistance of PQ Corporation, John Armor (Air Products), and Lynn Slaugh (Shell) in providing samples of zeolites. We also acknowledge James Hickenlooper, who aided in the FTIR experiments, and Victor Chao, who assisted in performing kinetic tests and surface area measurements carried out as portions of this study. We are grateful to Dr. William Hecker for useful discussions.

REFERENCES

1. Li, Y., and Armor, J. N., *Appl. Catal. B* **2**, 239 (1993).
2. Adelman, B. J., Lei, G. D., and Sachtler, W. M. H., *Catal. Lett.* **28**, 119 (1994).
3. Hamada, H., Kintaichi, Y., Sasaki, M., Ito, T., and Tabata, M., *Appl. Catal.* **64**, L1 (1990).
4. Li, Y., and Armor, J. N., *J. Catal.* **145**, 1 (1994).
5. Kiovsky, J. R., Koradia, P. B., and Lim, C. T., *I.E.C. Prod. Res. Dev.* **19**, 218 (1980).
6. Hamada, H., Kintaichi, Y., Sasaki, M., Ito, T., and Tabata, M., *Appl. Catal.* **70**, L15 (1991).
7. Sasaki, M., Hamada, H., Kintaichi, Y., and Ito, T., *Catal. Lett.* **15**, 297 (1992).
8. Yogo, K., Umeno, M., Watanabe, H., and Kikuchi, E., *Catal. Lett.* **19**, 131 (1993).
9. Cowan, A. D., Dumpelmann, R., and Cant, N. W., *J. Catal.* **151**, 356 (1995).
10. Komatsu, T., Nunokawa, M., Moon, I. S., Takahara, T., Namba, S., and Yashima, T. J., *J. Catal.* **148**, 427 (1994).
11. Li, Y., and Armor, J. N., *J. Catal.* **150**, 376 (1994).
12. Smits, R. H. H., and Iwasawa, Y., *Appl. Catal. B* **6**, L201 (1995).
13. Yokoyama, C., and Misono, M., *J. Catal.* **150**, 9 (1994).
14. Andersson, L. A. H., Brandin, J. G. M., and Odenbrand, C. U. I., *Catal. Today* **4**, 173 (1989).
15. Brandin, J. G. M., Andersson, L. A., and Odenbrand, C. U., *Catal. Today* **4**, 187 (1989).
16. Odenbrand, C. U. I., Andersson, L. A. H., Brandin, J. G. M., and Haras, S., *Catal. Today* **4**, 155 (1989).
17. Ito, E., Hultermans, R. J., Lugt, P. M., Burgers, M. H. W., Rigutto, M. S., van Bekkum, H., and van den Bleek, C. M., *Appl. Catal. B* **4**, 95 (1994).
18. Adelman, B. J., Beutel, T., Lei, G. D., and Sachtler, W. M. H., *J. Catal.* **158**, 327 (1996).
19. Cheung, T., Bhargava, S. K., Hobday, M., and Foger, K., *J. Catal.* **158**, 301 (1996).
20. Li, Y., and Armor, J. N., *J. Catal.* **150**, 388 (1994).
21. Eng, J., and Bartholomew, C. H., *J. Catal.* **171**, 14 (1997).
22. Eng, J., "Kinetics and Mechanism of Nitrogen Oxide Reduction with Ammonia over H-Form Zeolites," Ph.D. dissertation, Brigham Young University, 1996.
23. Nam, I. S., Eldridge, J. W., and Kittrell, J. R., *Stud. Surf. Sci. Catal.* **38**, 589 (1988).
24. Bagnasco, G., *J. Catal.* **159**, 249 (1996).
25. Kogelbauer, A., Lercher, J. A., Steinberg, K. H., Roessner, F., Soellner, A., and Dmitriev, R. V., *Zeolites* **9**, 224 (1989).
26. Teunissen, E. H., van Santen, R. A., Jansen, A. P. J., and Van Duijneveldt, F. B., *J. Phys. Chem.* **97**, 203 (1993).
27. Hidalgo, C. V., Itoh, H., Hattori, T., Niwa, M., and Murakami, Y., *J. Catal.* **85**, 362 (1984).
28. Crocker, M., Herold, R. H. M., Sonnemans, M. H. W., Emeis, C. A., Wilson, A. E., and van der Moolen, J. N., *J. Phys. Chem.* **97**, 432 (1993).
29. Chen, D. T., Sharma, S. B., Filimonov, I., and Dumesic, J. A., *Catal. Lett.* **12**, 201 (1992).
30. Haag, W. [Personal communications, 1995]

31. Valyon, J., and Hall, W. K., *J. Phys. Chem*. **97**, 1204 (1993).
32. Nakamoto, K., "Infrared Spectra of Inorganic and Coordination Compounds," Wiley–Interscience. New York, 1970.
33. Aylor, A. W., Lobree, L. J., Reimer, J. A., and Bell, A. T. [Unpublished manuscript]
34. Aylor, A. W., Larsen, S. C., Reimer, J. A., and Bell, A. T., *J. Catal.* **157**, 592 (1995).
35. Hoost, T. E., Laframboise, K. A., and Otto, K., *Appl. Catal. B* **7**, 79 (1995).
36. Williamson, W. B., and Lunsford, J. H., *J. Phys. Chem*. **80**, 2664 (1976).
37. Harrison, J. A., Maclagan, R. G. A. R., and Whyte, A. R., *J. Phys. Chem*. **91**, 6683 (1987).
38. Ebitani, K., Tsuji, J., Hattori, H., and Kita, H., *J. Catal.* **138**, 750 (1992).
39. Lercher, J. A., van Santen, R. A., and Vinek, H., *Catal. Lett.* **27**, 91 (1994).
40. Choi, E. Y., Nam, I. S., Kim, Y. G., Chung, J. S., and Lee, J. S., *J. Mol. Catal.* **69**, 247 (1991).
41. Ham, S. W., Choi, H., Nam, I. S., and Kim, Y. G., *Catal. Today* **11**, 611 (1992).